Physics-Informed Autoencoder for DSC-MRI Perfusion Post-Processing: Application to Glioma Grading

Pierre Fayolle, Alexandre Bône, Noëlie Debs, Mathieu Naudin, Pascal Bourdon, Rémy Guillevin, David Helbert

▶ **To cite this version:**

Pierre Fayolle, Alexandre Bône, Noëlie Debs, Mathieu Naudin, Pascal Bourdon, et al.. Physics-Informed Autoencoder for DSC-MRI Perfusion Post-Processing: Application to Glioma Grading. International Symposium on Biomedical Imaging (ISBI 2025), Institute of Electrical and Electronics Engineers (IEEE), Apr 2025, Houston (Texas), United States. hal-04872430

HAL Id: hal-04872430
https://hal.science/hal-04872430v1

Submitted on 4 Feb 2025

HAL is a multi-disciplinary open access archive for the deposit and dissemination of scientific research documents, whether they are published or not. The documents may come from teaching and research institutions in France or abroad, or from public or private research centers.

L'archive ouverte pluridisciplinaire **HAL**, est destinée au dépôt et à la diffusion de documents scientifiques de niveau recherche, publiés ou non, émanant des établissements d'enseignement et de recherche français ou étrangers, des laboratoires publics ou privés.

Physics-Informed autoencoder for DSC-MRI Perfusion post-processing: application to glioma grading

Pierre Fayolle[1,2,5,*] Alexandre Bône[1] Noëlie Debs[1] Mathieu Naudin[2,3,5]
Pascal Bourdon[4,5] Rémy Guillevin[2,3,5] David Helbert[4,5]

Abstract

DSC-MRI perfusion is a medical imaging technique for diagnosing and prognosing brain tumors and strokes. Its analysis relies on mathematical deconvolution, but noise or motion artifacts in a clinical environment can disrupt this process, leading to incorrect estimate of perfusion parameters. Although deep learning approaches have shown promising results, their calibration typically rely on third-party deconvolution algorithms to generate reference outputs and are bound to reproduce their limitations.

To adress this problem, we propose a physics-informed autoencoder that leverages an analytical model to decode the perfusion parameters and guide the learning of the encoding network. This autoencoder is trained in a self-supervised fashion without any third-party software and its performance is evaluated on a database with glioma patients. Our method shows reliable results for glioma grading in accordance with other well-known deconvolution algorithms despite a lower computation time. It also achieved competitive performance even in the presence of high noise which is critical in a medical environment.

DSC-MRI, Perfusion maps, Deconvolution, Physics-Informed Neural Networks, Glioma

1 Introduction

Dynamic Susceptibility Contrast Magnetic Resonance Imaging (DSC-MRI) perfusion is an MRI modality that involves the injection of a contrast agent that causes changes in magnetic susceptibility signals over time. These modifications can be quantified to generate perfusion maps, which are essential for radiologists to accurately diagnose brain tumors or strokes.

The perfusion parameters are typically obtained by deconvolution of the DSC signals with a reference signal, called arterial input function (AIF), measured in the main arteries irriguating the brain. Characteristics of the resulting tissue response function (TRF) are then derived to define perfusion maps such as the cerebral blood flow (CBF) and the mean transit time (MTT). To solve this ill-posed problem, various methods have been published relying on Singular Value Decomposition (SVD) [1, 2]. However, studies have found that these methods tend to underestimate CBF and may introduce non-physiological oscillations in TRF, even when regularization terms are applied [3].

Deep learning approaches have recently been proposed as an alternative, aiming to automatically generate perfusion maps by learning from third-party deconvolution algorithms as reference [4, 5, 6]. More recently, new methods that did not rely on third-party softwares to define reference labels have been published [7, 8]. Instead, they trained a physics-informed neural network with simulated data to solve the deconvolution. This approach outperformed other deconvolution algorithms, even with high noise images. Nonetheless, the simulations generate concentration curves that can be far from *in vivo* data.

In this paper, we propose a physics-informed autoencoder (PHAE) trained with *in vivo* data, that does not require any ground truth to perform the deconvolution and generate the perfusion maps with a high robustness to noise and a low computational cost. Distinguishing Low Grade Glioma (LGG) from High Grade Glioma (HGG) was used as a metric to evaluate the performance of the proposed method in comparison with standard deconvolution algorithms.

*Corresponding author (pierre.fayolle@univ-poitiers.fr)
[1] Guerbet Research, Villepinte, France
[2] LMA, Université de Poitiers, France
[3] CHU de Poitiers, Poitiers, France
[4] XLIM, Université de Poitiers, France
[5] I3M, Common Laboratory CNRS-Siemens, France

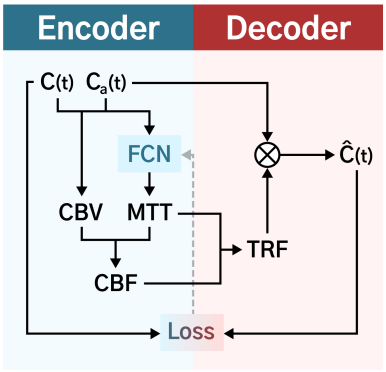

Figure 1: Workflow of the PHAE. $C(t)$: tissue concentration, $C_a(t)$: arterial concentration, FCN: Fully Convolutional Network, CBV: Cerebral Blood Volume, CBF: Cerebral Blood Flow, MTT: Mean Transit Time, TRF: Tissue Response Function. CBV is calculated from Eq. 2, CBF from Eq. 3, TRF from Eqs. 4-5, $\hat{C}(t)$ from Eq. 6.

2 Methods

2.1 Data

2.1.1 Public dataset

DSC-MRI sequences from 49 patients with glioma were collected from the public QIN-BRAIN-DSC-MRI dataset [9]. Among these subjects, 13 were histologically diagnosed with low-grade glioma (LGG) and 36 with high-grade glioma (HGG). Manually-defined tumor segmentation maps, normal-appearing white matter and arterial voxels were also retrieved. Arterial signals were then averaged to derive the patient-specific AIF.

2.1.2 Private dataset

Additionally, DSC-MRI sequences acquired from 15 patients at Poitiers University Hospital were collected, including 8 LGG and 7 HGG patients confirmed by biopsy. Imaging sequences were acquired with a 3T MRI machine (Skyra, Siemens Healthineers). AIF extraction, tumor and normal-appearing white matter segmentations were performed by radiologists.

2.1.3 Data split and preprocessing

From the public dataset, 39 patients were assigned to the train set. All 25 remaining patients were assigned to the test set. All signals over time were extracted from the DSC-MRI images and transformed into concentration-time-curve $C(t)$ with the following equation:

$$C(t) = -\frac{1}{TE} \ln\left(\frac{S(t)}{S_0}\right) \tag{1}$$

where TE is the echo time, $S(t)$ is the DSC signal over time and S_0 is the DSC signal baseline. $C(t)$ and $C_a(t)$ (also named as AIF) were normalized between 0 and 1, by dividing all the curves by the maximum value found for each subject.

2.2 Physics-informed autoencoder (PHAE)

The proposed PHAE method is presented in Fig. 1. This model is divided into an encoder that generates the perfusion parameters and a decoder that ensures the reliabilty of the perfusion parameters by reconstructing $C(t)$.

Methods	AUC	Cut-off value	Sensitivity (%)	Specificity (%)	Accuracy (%)	Inference time (s)
oSVD [2]	0.87 (0.69-0.99)	1.77 (1.04-2.25)	69.2 (50.0-100.0)	100.0 (69.2-100.0)	84.0	11.8 (7.09-17.33)
Tikhonov [10]	0.88 (0.71-1.00)	1.75 (1.01-1.95)	69.2 (53.8-100.0)	100.0 (75.0-100.0)	84.0	33.6 (16.31-51.44)
PHAE (ours)	**0.90** (0.74-1.00)	1.18 (1.05-1.40)	**76.9** (59.9-100.0)	100.0 (84.6-100.0)	**88.0**	**8.4** (3.82-13.01)

Table 1: Diagnostic performance and computational time cost of CBF maps for differenciating LGG from HGG. Data in parenthesis represent the 95% confidence intervals. The inference time represents the average time to process a single patient.

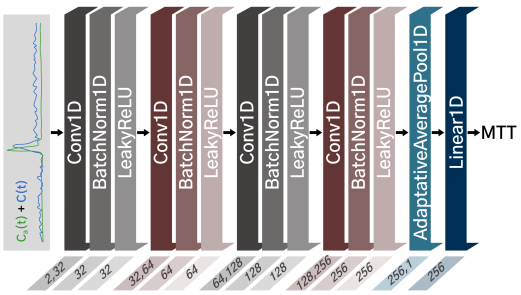

Figure 2: Architecture of the Fully Convolutional Network (FCN). Values represent the layer parameters.

2.2.1 Deep encoding network

Fig. 2 details the architecture of the proposed 1D Fully Convolutional Network (FCN). It takes as input a pair of $C(t)$ and $C_a(t)$. These inputs are fed into 4 blocks having each an 1D convolutional layer, an 1D batch normalization, a leaky ReLU with a negative slope of 0.02. The number of extracted feature maps is set to 32 and is multiplied by 2 for each following convolutional block. The kernel size is set to 3 with a stride and a padding of 1 for each block. Then, an 1D average pooling is followed by a final linear layer with a single value as output corresponding to MTT. In the other hand, CBV is calculated by integrating $C(t)$ over $C_a(t)$ as followed:

$$CBV = \frac{\int_0^\infty C(t)\,dt}{\int_0^\infty C_a(t)\,dt} \quad \left[\frac{ml}{100g}\right] \tag{2}$$

CBV are divided by the generated MTT to calculate CBF according to the central volume theorem

$$CBF = \frac{CBV}{MTT} \quad \left[\frac{ml}{100g \cdot min}\right] \tag{3}$$

Here, MTT is the only perfusion parameters that is generated by the encoder as the CBV can be calculated beforehand, and the CBF can be computed through the previous equation to simplify the model.

2.2.2 Physics-informed decoder

To ensure the reliability of MTT values, a physics-informed decoder was developed based on the perfusion equations and using the previously generated perfusion parameters as input. From MTT, a simulation of the residual function $R(t)$ is done using Lorentzian equation as proposed in [10]:

$$R(t) = \frac{1}{1 + \left(\frac{\pi \cdot t}{2 \cdot MTT}\right)^2} \tag{4}$$

Using a simulation for the generation of $R(t)$ is here to ensure a realistic shape without unwanted oscillations that could impact perfusion parameter estimate. The residual function is multiplied by CBF to obtain TRF:

$$TRF = R(t) \cdot CBF \tag{5}$$

Then, TRF is convolved with $C_a(t)$ to reconstruct a new $\hat{C}(t)$ according to the following equation:

$$\hat{C}(t) = C_a(t) \otimes TRF \tag{6}$$

2.2.3 Training details

The more realistic the generated MTT values, the closer the $\hat{C}(t)$ reconstuctions match $C(t)$. Therefore, the mean absolute error was used as a loss between $C(t)$ and $\hat{C}(t)$ to constrain the encoder in the possible MTT values to generate. The encoder was trained during 65 epochs in approximatively 37 minutes. The ADAM optimization algorithm was used with a learning rate of 0.0001 and without weight decay. The batch size was set to 1536.

2.3 Experimental setup

To generate perfusion maps for the test dataset, $C(t)$ and $C_a(t)$ of each patient were sent to the encoder only. This results in a MTT value for each voxel of the brain, converting the 4D time series into a 3D image. To evaluate the performance of our approach in generating MTT and thus CBF maps (via Eq. 3), two baseline deconvolution methods were used, oSVD [2] and Tikhonov [10] as implemented in [11].

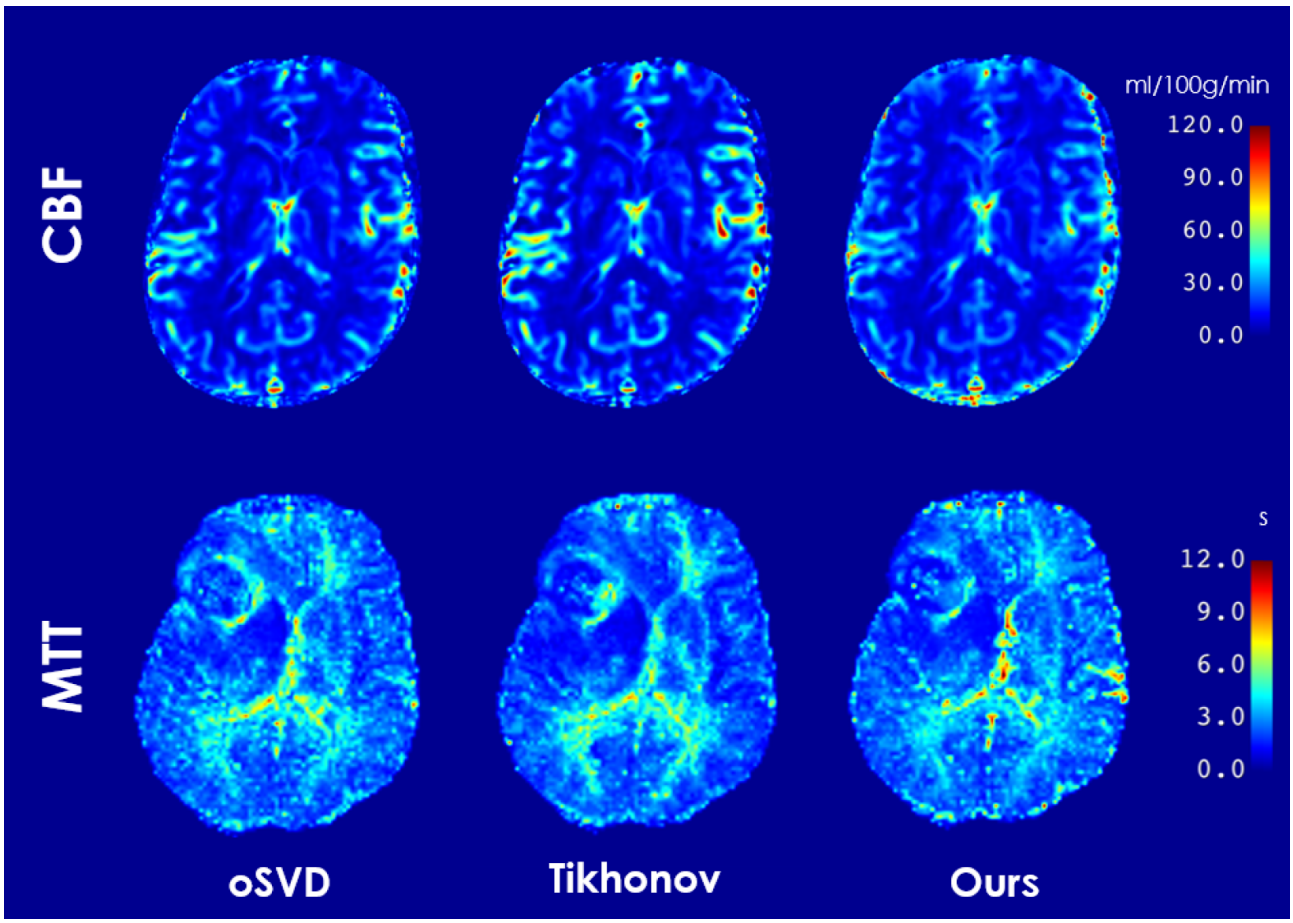

Figure 3: Comparison of CBF maps (grade 2 glioma) and MTT maps (grade 4 glioma) generated by oSVD [2], Tikhonov [10] and our methods.

By computing the mean CBF values of a lesion Region Of Interest (ROI) divided by the mean CBF values of a healthy ROI contralateral of the lesion, a ratio can be obtained. This ratio can be used to determine glioma grading [12]. For that purpose, both tumor and normal-appearing white matter segmentations were used to calculate the ratio for each patient.

Receiver Operating Characteristic curve (ROC) analysis was used with Area Under the Curve (AUC) to quantify classification accuracy. A cut-off ratio to distinguish LGG from HGG was then estimated for each method by maximizing both sensitivity and specificity with Youden's method [13].

To evaluate the robustness to noise, test dataset signals were progressively degraded from an SNR of 50 to 10. $C_a(t)$ signals were systematically recomputed from the degraded DSC sequences. The SNR was calculated as the mean of the DSC signal baseline divided by its standard deviation. Gaussian noise was added to achieve specified SNR values.

3 Results

3.1 Qualitative results

The generated CBF and MTT maps are shown in Fig. 3. The PHAE method maps are visually close from oSVD and Tikhonov methods. The majority of variations in both CBF and MTT maps originate from gray matter and cerebrospinal fluid, with several outlier values observed across each method.

3.2 Glioma grading performance

Results of deconvolution methods (oSVD, Tikhonov, and the PHAE) for generating the CBF maps are summarized in Table 1. The AUC were closely similar with respectively 0.87 (0.69-0.99), 0.88 (0.71-1.00) and 0.90 (0.74-1.00). The accuracies for distinguishing LGG from HGG are 84% (21 subjects correctly classified) for oSVD and Tikhonov, and 88% (22 subjects correctly classified) for the proposed PHAE method. Fig. 4 shows boxplots categorized by glioma grading. The PHAE method showed less spread CBF values for LGG. The

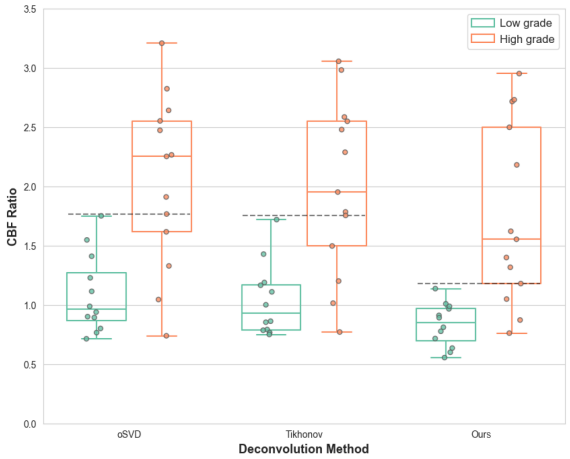

Figure 4: Boxplots for each deconvolution methods based on CBF ratio to distinguish Low Grade Glioma (LGG) from High Grade Glioma (HGG). Each point represents a subject. The dashed lines represent the optimal cut-off values for the respective deconvolution methods.

Mann-Whitney U test was employed to compare the distributions between LGG and HGG groups for each method. As a result, statistically significant differences was found, with p-values of 0.007, 0.003, and 0.0009 for oSVD, Tikhonov, and PHAE respectively.

3.3 Robustness to noise evaluation

After adding Gaussian noise, the ROC curves and AUC values were computed for each SNR level. Fig. 5 shows the AUC values of each deconvolution method to distinguish LGG from HGG as the SNR decreases. As expected, artificially reducing the SNR tends to decrease the performance of each method. The PHAE method outperforms oSVD and Tikhonov algorithms even under high noise levels (low SNR).

3.4 Computational performance

The inference time was measured (Intel Xeon Platinum 8253 CPU and 192GB RAM) for the generation of both MTT and CBF maps and were respectively 11.8 (7.09-17.33), 33.6 (16.31-51.44) and 8.4 (3.82-13.01) seconds on average per patient.

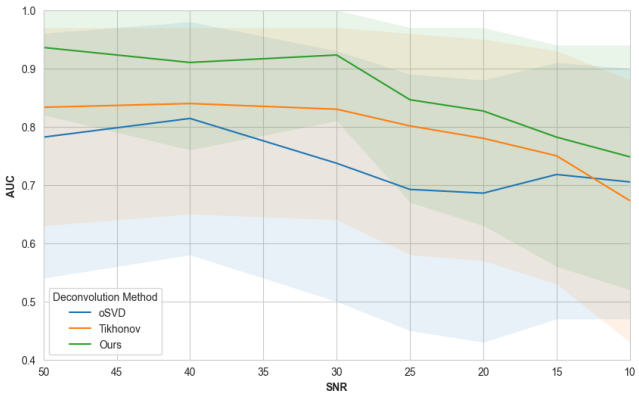

Figure 5: AUC values with their confidence intervals as a function of SNR estimated for each deconvolution method.

4 Discussion

The proposed PHAE method demonstrated performance comparable to the oSVD and Tikhonov methods in differentiating LGG from HGG. Interestingly, this confirms the feasibility of the proposed approach to learn to estimate the perfusion parameters without the need of third-party references. Although CBF ratio cut-off threshold of our method are lower than others, it did not impact the quality of the resulting maps.

Among the test dataset, 4 patients were histologically diagnosed as grade 3 according to the WHO 2016 classification [14]. All three methods failed to classify these glioma cases as HGG. The tumor segmentations showed indeed lower CBF values, even though higher values would be expected. Hypothetically, this could be explained either by an inaccurate segmentation of the active tumor core, or by a presence of LGG site in this segmentation, lowering CBF values.

The standard deconvolution methods require a longer processing time to generate the perfusion maps. To expedite this process, a compromise is often reached and leads to an increase estimating errors for the generated maps [7]. In contrast, the PHAE method can generate the perfusion maps in less than 9 seconds per subject, that is crucial for clinical applications to speed up diagnosis and preventive measures.

In the literature, multiple studies worked on simulating the residual function or TRF as proposed in [10]. In this work, the Lorentzian simulation function was chosen. Interestingly, no significative change was found for mono-exponential, gamma function and Lorentzian function. Other simulation functions such as bi-exponential, Fermi function or vascular model were not tested as they are not directly generated by MTT and result in a more complex model that was not the purpose of this work.

Despite the reliable generation of both CBF and MTT, the DSC perfusion parameter T_{max} was not generated. Including this parameter in the PHAE may faciliate the generation of more accurate $\hat{C}(t)$ and will be one of the main focus of our future work.

5 Conclusion

In summary, this paper presents a new approach for the perfusion parameter generation in DSC-MRI perfusion. We proposed a physics-informed autoencoder that estimates reliable CBF and MTT in accordance with other standard deconvolution methods without any third-party perfusion maps used as reference. The PHAE method showed better results for distinguishing LGG from HGG even in high presence of noise while needing less time to generate perfusion maps.

6 Acknowledgments

P.F., A.B., and N.D. are employees of Guerbet. This work was supported by ANRT (CIFRE 2023/1206).

7 Compliance with Ethical Standards

The private dataset comes from a study performed in accordance with the ethical standards as laid down in the 2013 Declaration of Helsinki. All patients approved the use of their data with a written consent.

References

[1] Leif Østergaard, Robert M Weisskoff, David A Chesler, Carsten Gyldensted, and Bruce R Rosen, "High resolution measurement of cerebral blood flow using intravascular tracer bolus passages. part i: Mathematical approach and statistical analysis," *Magnetic resonance in medicine*, vol. 36, no. 5, pp. 715–725, 1996.

[2] Ona Wu, Leif Østergaard, Robert M Weisskoff, Thomas Benner, Bruce R Rosen, and A Gregory Sorensen, "Tracer arrival timing-insensitive technique for estimating flow in mr perfusion-weighted imaging using singular value decomposition with a block-circulant deconvolution matrix," *Magnetic Resonance in Medicine: An Official Journal of the International Society for Magnetic Resonance in Medicine*, vol. 50, no. 1, pp. 164–174, 2003.

[3] Amit Mehndiratta, Bradley J MacIntosh, David E Crane, Stephen J Payne, and Michael A Chappell, "A control point interpolation method for the non-parametric quantification of cerebral haemodynamics from dynamic susceptibility contrast mri," *Neuroimage*, vol. 64, pp. 560–570, 2013.

[4] King Chung Ho, Fabien Scalzo, Karthik V Sarma, Suzie El-Saden, and Corey W Arnold, "A temporal deep learning approach for mr perfusion parameter estimation in stroke," in *2016 23rd International Conference on Pattern Recognition (ICPR)*. IEEE, 2016, pp. 1315–1320.

[5] Tabea Kossen, Vince I Madai, Matthias A Mutke, Anja Hennemuth, Kristian Hildebrand, Jonas Behland, Cagdas Aslan, Adam Hilbert, Jan Sobesky, Martin Bendszus, et al., "Image-to-image generative adversarial networks for synthesizing perfusion parameter maps from dsc-mr images in cerebrovascular disease," *Frontiers in Neurology*, vol. 13, pp. 1051397, 2023.

[6] Salmonn Talebi, Siyu Gai, Aaron Sossin, Vivian Zhu, Elizabeth Tong, and Mohammad RK Mofrad, "Deep learning for perfusion cerebral blood flow (cbf) and volume (cbv) predictions and diagnostics," *Annals of Biomedical Engineering*, vol. 52, no. 6, pp. 1568–1575, 2024.

[7] Muhammad Asaduddin, Eung Yeop Kim, and Sung-Hong Park, "Spinned: Simulation-based physics-informed neural network for deconvolution of dynamic susceptibility contrast mri perfusion data," *Magnetic Resonance in Medicine*, 2024.

[8] Lukas T Rotkopf, Christian H Ziener, Nikolaus von Knebel-Doeberitz, Sabine D Wolf, Anja Hohmann, Wolfgang Wick, Martin Bendszus, Heinz-Peter Schlemmer, Daniel Paech, and Felix T Kurz, "A physics-informed deep learning framework for dynamic susceptibility contrast perfusion mri," *Medical physics*, 2024.

[9] Kathleen M Schmainda, Melissa A Prah, Jennifer M Connelly, and Scott D Rand, "Glioma dsc-mri perfusion data with standard imaging and rois," *The Cancer Imaging Archive. http://doi. org/10.7937 K*, vol. 9, 2016.

[10] Fernando Calamante, David G Gadian, and Alan Connelly, "Quantification of bolus-tracking mri: improved characterization of the tissue residue function using tikhonov regularization," *Magnetic Resonance in Medicine: An Official Journal of the International Society for Magnetic Resonance in Medicine*, vol. 50, no. 6, pp. 1237–1247, 2003.

[11] Sabela Fernández-Rodicio, Gonzalo Ferro-Costas, Ana Sampedro-Viana, Marcos Bazarra-Barreiros, Alba Ferreirós, Esteban López-Arias, María Pérez-Mato, Alberto Ouro, José M Pumar, Antonio J Mosqueira, et al., "Perfusion-weighted software written in python for dsc-mri analysis," *Frontiers in Neuroinformatics*, vol. 17, pp. 1202156, 2023.

[12] Bahattin Hakyemez, C Erdogan, I Ercan, N Ergin, S Uysal, and S Atahan, "High-grade and low-grade gliomas: differentiation by using perfusion mr imaging," *Clinical radiology*, vol. 60, no. 4, pp. 493–502, 2005.

[13] Marcus D Ruopp, Neil J Perkins, Brian W Whitcomb, and Enrique F Schisterman, "Youden index and optimal cut-point estimated from observations affected by a lower limit of detection," *Biometrical Journal: Journal of Mathematical Methods in Biosciences*, vol. 50, no. 3, pp. 419–430, 2008.

[14] David N Louis, Arie Perry, Guido Reifenberger, Andreas Von Deimling, Dominique Figarella-Branger, Webster K Cavenee, Hiroko Ohgaki, Otmar D Wiestler, Paul Kleihues, and David W Ellison, "The 2016 world health organization classification of tumors of the central nervous system: a summary," *Acta neuropathologica*, vol. 131, pp. 803–820, 2016.